Supporting Information for

A series of climate oscillations around 8.2 ka BP revealed through multi-proxy speleothem records from North China

Pengzhen Duan[1], Hanying Li[2], Zhibang Ma[3], Jingyao Zhao[2], Xiyu Dong[2], Ashish Sinha[4], Peng Hu[5,6], Haiwei Zhang[2], Youfeng Ning[2], Guangyou Zhu[1], Hai Cheng[2,7,8]

[1]Research Institute of Petroleum Exploration and Development, PetroChina, Beijing, China

[2]Institute of Global Environmental Change, Xi'an Jiaotong University, Xi'an, China

[3]Key Laboratory of Cenozoic Geology and Environment, Institute of Geology and Geophysics, Chinese Academy of Sciences, Beijing, China

[4]Department of Earth Science, California State University, Dominguez Hills, Carson, USA

[5]Yunnan Key Laboratory of Meteorological Disasters and Climate Resources in the Greater Mekong Subregion, Yunnan University, Kunming 650091, China

[6]Department of Atmospheric Sciences, Yunnan University, Kunming 650500, China

[7]State Key Laboratory of Loess and Quaternary Geology, Institute of Earth Environment, Chinese Academy of Sciences, Xi'an, China

[8]Key Laboratory of Karst Dynamics, MLR, Institute of Karst Geology, CAGS, Guilin, China

Correspondence to: Hanying Li (hanyingli@xjtu.edu.cn) and Hai Cheng (cheng021@xjtu.edu.cn)

Contents of this file

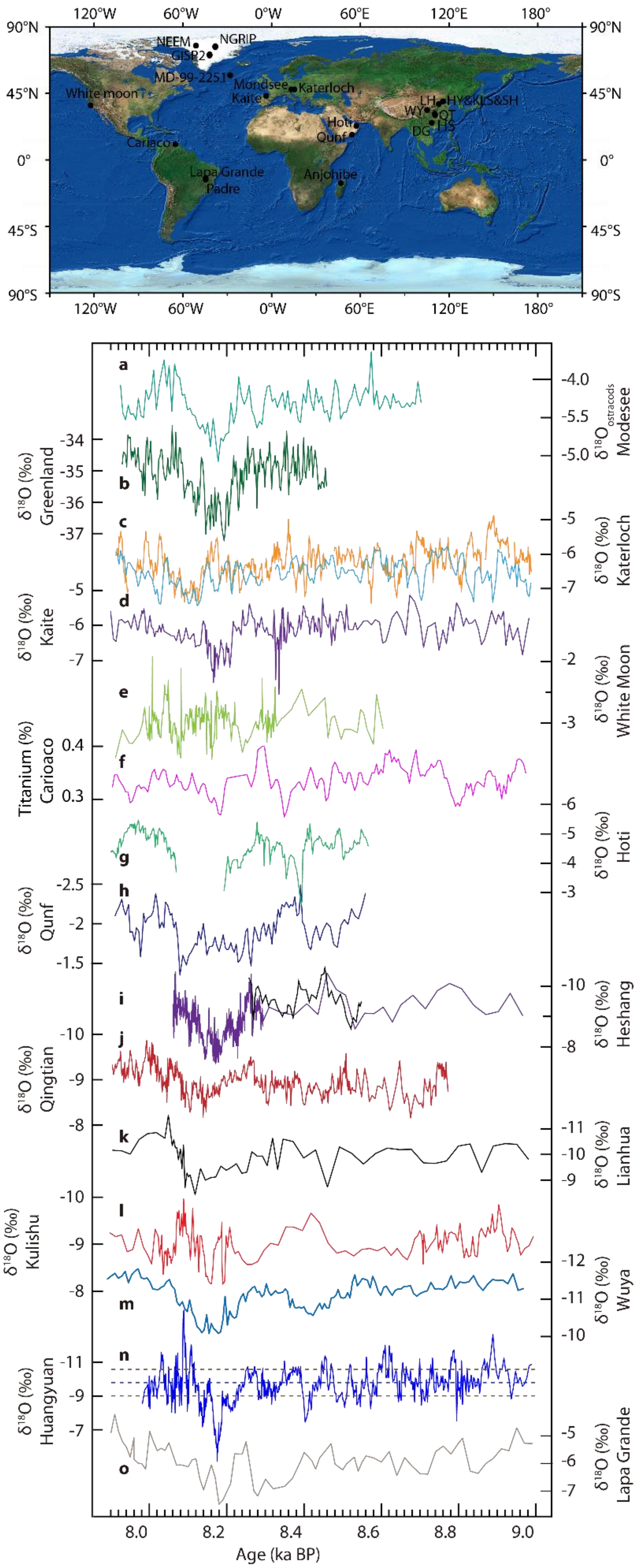

120°W
60°W
0°W
60°E
120°E
180°
90°N
45°N
0°
45°S
90°S
NEEM
NGRIP
GISP2
MD-99-2251
Mondsee
Katerloch
Kaite
White moon
Hoti
Qunf
LH
HY&KLS&SH
WY
QT
DG
HS
Cariaco
Lapa Grande
Padre
Anjohibe
a
b
c
d
e
f
g
h
i
j
k
l
m
n
o
δ18O ostracods Modesee
δ18O (‰) Greenland
δ18O (‰) Katerloch
δ18O (‰) Kaite
δ18O (‰) White Moon
Titanium (%) Carioaco
δ18O (‰) Hoti
δ18O (‰) Qunf
δ18O (‰) Heshang
δ18O (‰) Qingtian
δ18O (‰) Lianhua
δ18O (‰) Kulishu
δ18O (‰) Wuya
δ18O (‰) Huangyuan
δ18O (‰) Lapa Grande
Age (ka BP)
8.0
8.2
8.4
8.6
8.8
9.0

Figure S1. Comparison between speleothem BH-2 $\delta^{18}O$ and other records during 9.0–7.9 ka BP. The black dots in the world map represent the proxy locations mentioned in our main text. (**a**) $\delta^{18}O_{ostracods}$ record from Modesee, Austria (Andersen et al., 2017). (**b**) Composite $\delta^{18}O$ record from Greenland ice core (Thomas et al., 2007). (**c**) $\delta^{18}O$ records (blue: K1, yellow: K3) from Katerloch Cave, Austria (Boch et al., 2009). (**d**) $\delta^{18}O$ record of speleothem LV5 from Kaite Cave, Spain (Domínguez-Villar et al., 2009). (**e**) Speleothem $\delta^{18}O$ record from White Moon Cave, California, America (Oster et al., 2017). (**f**) Bulk Titanium content of Cariaco Basin sediments from ODP Site 1002 (Huag et al., 2002). (**g**) Speleothem $\delta^{18}O$ record from Hoti Cave, Oman (Cheng et al., 2009). (**h**) High-resolution $\delta^{18}O$ record from Qunf Cave, Oman (Fleitmann et al., 2003; Cheng et al., 2009) based on more precise ^{230}Th dating results (Cheng et al., 2009). (**i–n**) Asian monsoon speleothem $\delta^{18}O$ records from Heshang Cave (Liu et al., 2013; Hu et al., 2008), Qingtian Cave (Liu et al., 2015), Lianhua Cave (Dong et al., 2018), Kulishu Cave (Duan W et al., 2021), Wuya Cave (Tan et al., 2020), and Huangyuan Cave (this study). The horizontal blue and purple dashed lines in the Huangyuan Cave record represent its mean and $\pm 1\sigma$ values, respectively. (**o**) Speleothem $\delta^{18}O$ record from Lapa Grande Cave, Brazil (Stríkis et al., 2011). The speleothem $\delta^{18}O$ scales in **c**, **d,** and **o** are inverse to other speleothem records.

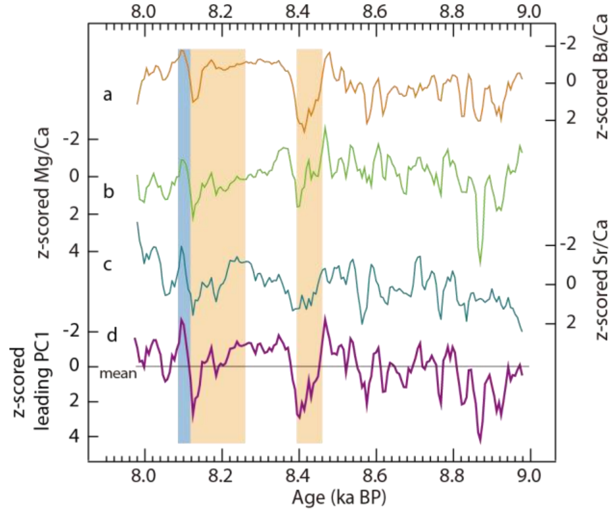

Figure S2. 30-year loess filtered *z*-scored trace element ratio results. (**a–d**) are Ba/Ca, Mg/Ca, Sr/Ca, and their leading PC records, respectively. The mean value of the PC1 record is indicated by the horizontal black line. The vertical yellow bars in the right subpanel mark the anomalously positive episodes and the light blue bar indicates the subsequent $\delta^{18}O$ overshoot after the 8.2 ka event same as the **Figure 2**.

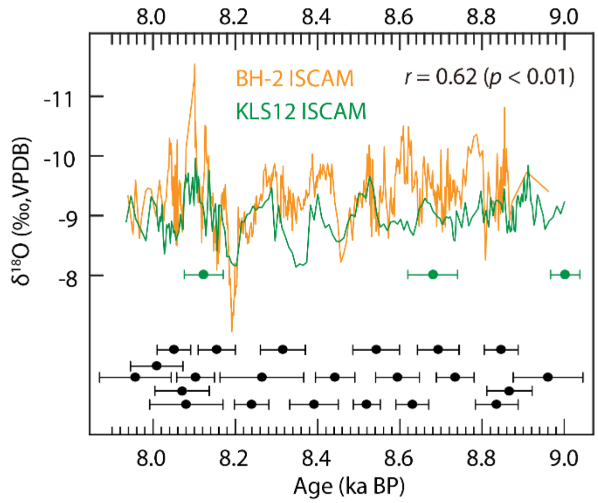

Figure S3. Replication test. ISCAM age model was used to reconstruct speleothems BH-2 (orange) and KLS12 (green) (Duan W et al., 2021) chronologies and $\delta^{18}O$ records. The correlation coefficient (*r*) between them is 0.62 at 99 % confidence level in their contemporary growth period. The ^{230}Th dates with 2σ analytical errors (green for KLS12 and black for BH-2) are presented for each speleothem record.

Table S1. ^{230}Th dating results for the BH-2. The error is at 2σ level.

Sample Number	depth (mm)	^{238}U (ppb)	^{232}Th (ppt)	^{230}Th / ^{232}Th (atomic x10^{-6})	$\delta^{234}U$* (measured)	^{230}Th / ^{238}U (activity)	^{230}Th Age (yr) (uncorrected)	^{230}Th Age (yr BP)*** (corrected)	$\delta^{234}U_{Initial}$** (corrected)
BH-2-1(1)	4	111.7 ±0.1	373 ±8	544 ±12	537.0 ±2.4	0.1102 ±0.0010	8080 ±75	7956 ±87	549 ±2
BH-2-T	7	90.6 ±0.1	322 ±6	513 ±11	531.0 ±1.8	0.1105 ±0.0006	8134 ±43	8008 ±64	543 ±2
BH-2-2	13	110.9 ±0.2	103 ±3	1970 ±60	542.7 ±3.1	0.1113 ±0.0012	8130 ±38	8050±41	555 ±3
BH-2-2(1)	18	114.2 ±0.1	164 ±3	1293 ±30	535.1 ±2.9	0.1128 ±0.0009	8158 ±65	8070 ±66	548 ±3
BH-2-3	24	125.1 ±0.1	117 ±3	1961 ±59	535.9 ±2.0	0.1113 ±0.0006	8160 ±45	8080 ±89	549 ±2
BH-2-3a	26	103.6 ±0.2	86 ±2	2210 ±49	530.8 ±2.1	0.1112 ±0.0006	8181 ±44	8103 ±46	543 ±2
BH-2-4	31	122.4±0.2	54 ±2	4158 ±92	527.2 ±2.5	0.1118 ±0.0006	8234 ±44	8154 ±45	540 ±3
BH-2-4a	34	121.8 ±0.2	90 ±2	2492 ±55	523.4 ±2.2	0.1123 ±0.0005	8315 ±41	8239 ±42	536 ±2
BH-2-4b	36	99.2 ±0.1	225 ±13	828 ±49	528.3 ±2.2	0.1138 ±0.0014	8400 ±98	8264 ±102	541 ±2
BH-2-5	38	102.4 ±0.1	213 ±4	905 ±19	527.1 ±2.5	0.1142 ±0.0006	8416 ±47	8315 ±55	540 ±3
BH-2-6	43	111.8 ±0.2	290 ±6	735.8±16	534.7 ±2.6	0.1159 ±0.0005	8503 ±57	8391 ±59	548 ±2
BH-2-7	48	121.8 ±0.2	57 ±2	3220 ±70	539.4 ±2.0	0.1166 ±0.0011	8513 ±88	8442 ±48	554 ±3
BH-7a	58	134.5 ±0.2	61 ±1	4272 ±94	538.1 ±1.9	0.1170 ±0.0004	8589 ±32	8519 ±33	551 ±2
BH-2-8	70	140.8 ±0.2	357 ±7	765 ±16	536.6 ±2.8	0.1177 ±0.0006	8651 ±46	8542 ±57	550 ±3
BH-2-9	86	128.7 ±0.2	85 ±2	2942 ±70	533.4 ±2.3	0.1177 ±0.0007	8668 ±52	8594 ±53	547 ±2
BH-9a	96	117.5 ±0.2	82 ±2	2781 ±61	533.0 ±2.1	0.1181 ±0.0005	8705 ±39	8630 ±40	546 ±2
BH-2-10	111	135.9 ±0.2	66 ±2	4031 ±101	529.5 ±2.6	0.1186 ±0.0006	8765 ±51	8693 ±51	543 ±3
BH-2-11	127	151.4 ±0.2	95 ±2	3109 ±70	525.3 ±2.0	0.1189 ±0.0006	8808 ±45	8734 ±46	538 ±2
BH-2-11a	137	139.7 ±0.2	97 ±2	2863 ±63	532.9 ±2.2	0.1209 ±0.0005	8921 ±40	8846 ±41	546 ±2
BH-2-12	149	137.2 ±0.2	74 ±2	3657 ±89	522.4 ±2.6	0.1199 ±0.0006	8907 ±52	8835 ±52	536 ±3
BH-2-13	164	151.0 ±0.2	178 ±4	1696 ±37	531.5 ±2.4	0.1212 ±0.0007	8950 ±53	8866 ±55	545 ±2
BH-2-14	167	138.9 ±0.2	120 ±3	2345 ±63	537.8 ±2.8	0.1229 ±0.0011	9039 ±84	8960 ±85	552 ±3

U decay constants: λ_{238} = 1.55125x10^{-10} and λ_{234} = 2.82206x10^{-6}. Th decay constant: λ_{230} = 9.1705x10^{-6}.

*$\lambda^{234}U$ = ([^{234}U/^{238}U] $_{activity}$ – 1) x 1000. **$\delta^{234}U_{initial}$ was calculated based on ^{230}Th age (T), i.e., $\lambda^{234}U_{initial}$ =$\lambda^{234}U_{measured}$ x eλ^{234xT}.

Corrected ^{230}Th ages assume the initial $^{230}Th/^{232}Th$ atomic ratio of 4.4 ±2.2 x10^{-6}. Those are the values for a material at secular equilibrium, with the bulk earth $^{232}Th/^{238}U$ value of 3.8. The errors are arbitrarily assumed to be 50 %.

***B.P. stands for "Before Present" where the "Present" is defined as the year 1950 A.D..

References

Andersen, N., Lauterbach, S., Erlenkeuser, H., Danielopol, D. L., Namiotko, T., and Hüls, M.: Evidence for higher-than-average air temperatures after the 8.2 ka event provided by a Central European $\delta^{18}O$ record, Quat. Sci. Rev., 172, 96–108. http://dx.doi.org/10.1016/j.quascirev.2017.08.001, 2017.

Boch, R., Spötl, C., and Kramers, J.: High-resolution isotope records of early Holocene rapid climate change from two coeval stalagmites of Katerloch Cave, Austria, Quat. Sci. Rev., 28, 2527–2538. https://doi.org/10.1016/j.quascirev.2009.05.015, 2009.

Cheng, H., Edwards, R. L., Shen, C. C., Polyak, V. J., Asmerom, Y., and Woodhead, J.: Improvements in ^{230}Th dating, ^{230}Th and ^{234}U half-life values, and U-Th isotopic measurements by multi-collector inductively coupled plasma mass spectrometry, Earth Planet Sci Lett, 371–372, 82–91. https://doi.org/10.1016/j.epsl.2013.04.006, 2013.

Cheng, H., Fleitmann, D., Edwards, R. L., Wang, X., Cruz, F. W., and Auler, A. S.: Timing and structure of the 8.2 kyr B.P. event inferred from $\delta^{18}O$ records of stalagmites from China, Oman, and Brazil, Geology, 37, 1007–1010. https://doi.org/10.1130/G30126A.1, 2009.

Domínguez-Villar, D., Fairchild, I. J., Baker, A., Wang, X., Edwards, R. L., and Cheng, H.: Oxygen isotope precipitation anomaly in the North Atlantic region during the 8.2 ka event, Geology, 37, 1095–1098. https://doi.org/10.1130/G30393A.1, 2009.

Dong, J., Shen, C. C., Kong, X., Wu, C. C., Hu, H. M., Ren, H., and Wang, Y.: Rapid retreat of the East Asian summer monsoon in the middle Holocene and a millennial weak monsoon interval at 9 ka in northern China, J. Asian. Earth. Sci., 151, 31–39. https://doi.org/10.1016/j.jseaes.2017.10.016, 2018.

Duan, P., Li, H., Sinha, A., Voarintsoa, N. R. G., Kathayat, G., Hu, P, and Cheng, H.: The timing and structure of the 8.2 ka event revealed through high-resolution speleothem records from northwestern Madagascar, Quat. Sci. Rev., 268, 107104. https://doi.org/10.1016/j.quascirev.2021.107104, 2021.

Duan, W., Ma, Z., Tan, M., Cheng, H., Edwards, R. L., and Wen, X.: Timing and structure of early-Holocene climate anomalies inferred from north Chinese stalagmite records, Holocene, 31, 1777–1785. https://doi.org/10.1177/09596836211033218, 2021.

Fleitmann, D., Burns, S. J., Mudelsee, M., Neff, U., Kramers, J., Mangini, A., and Matter, A.: Holocene forcing of the Indian monsoon recorded in a stalagmite from southern Oman, Science, 300, 1737–1739. https://doi.org/10.1126/science.1083130, 2003.

Hu, C., Henderson, G. M., Huang, J., Xie, S., Sun, Y., and Johnson, K. R. Quantification of Holocene Asian monsoon rainfall from spatially separated cave records, Earth Planet. Sci. Lett., 266, 221–232. https://doi.org/10.1016/j.epsl.2007.10.015, 2008.

Kobashi, T., Menviel, L., Jeltsch-Thömmes, A., Vinther, B. M., Box, J. E., and Muscheler, R.: Volcanic influence on centennial to millennial Holocene Greenland temperature change, Sci. Rep., 7, 1–10. https://doi.org/10.1038/s41598-017-01451-7, 2017.

Liu, D., Wang, Y., Cheng, H., Edwards, R. L., and Kong, X.: Cyclic changes of Asian monsoon intensity during the early mid-Holocene from annually-laminated stalagmites, central China, Quat. Sci. Rev., 121, 1–10. https://doi.org/10.1016/j.quascirev.2015.05.003, 2015.

Liu, Y. H., Henderson, G. M., Hu, C. Y., Mason, A. J., Charnley, N., and Johnson, K. R.: Links between the East Asian monsoon and north Atlantic climate during the 8,200 year event, Nat. Geosci., 6, 117–120. https://doi.org/10.1038/ngeo1708, 2013.

Oster, J. L., Sharp, W. D., Covey, A. K., Gibson, J., Rogers, B., and Mix, H. Climate response to the 8.2 ka event in coastal California, Sci. Rep., 7, 1–9. https://doi.org/10.1038/s41598-017-04215-5, 2017.

Stríkis, N. M., Cruz, F. W., Cheng, H., Karmann, I., Edwards, R. L., and Vuille, M. Abrupt variations in South American monsoon rainfall during the Holocene based on a speleothem record from central-eastern Brazil, Geology, 39, 1075–1078. https://doi.org/10.1130/G32098.1, 2011.

Tan, L., Li, Y., Wang, X., Cai, Y., Lin, F., Cheng, H., Ma, L., Sinha, A., and Edwards, R. L. Holocene monsoon change and abrupt events on the western Chinese Loess Plateau as revealed by accurately dated stalagmites, Geophys. Res. Lett., 47, e2020GL090273. https://doi.org/10.1029/2020GL090273, 2020.

Thomas, E. R., Wolff, E. W., Mulvaney, R., Steffensen, J. P., Johnsen, S. J., and Arrowsmith, C. The 8.2 ka event from Greenland ice cores, Quat. Sci. Rev., 26, 70–81. https://doi.org/10.1016/j.quascirev.2006.07.017, 2007.